JOURNAL OF Materials CHEMISTRY

Fabrication and characterization of Pt nanoparticles dispersed in Nb_2O_5 composite films by liquid phase deposition

Hnin Yu Yu Ko,[a] Minoru Mizuhata,[b] Akihiko Kajinami[b] and Shigehito Deki*[b]

[a]*Division of Molecular Science, The Graduate School of Science and Technology, Kobe University, Rokkodai, Nada, Kobe 657-8501, Japan*
[b]*Department of Chemical Science and Engineering, Faculty of Engineering, Kobe University, Rokkodai, Nada, Kobe 657-8501, Japan. E-mail: deki@kobe-u.ac.jp; Fax: +81(78)-803-6160; Tel: +81(78)-803-6160*

Received 20th November 2001, Accepted 4th March 2002
First published as an Advance Article on the web 2nd April 2002

Pt nanoparticle-doped Nb_2O_5 composite films ($\sim$80 nm thickness) have been prepared by the liquid phase deposition method. The deposited films were characterized by X-ray diffraction (XRD), high-resolution transmission electron microscopy (HRTEM), X-ray photoelectron spectroscopy (XPS) and Fourier transform infrared spectroscopy (FT-IR). Heat treatment of the deposited films above 200 °C under airflow produced dispersion of the Pt particles. The mean sizes of the Pt particles varied from 2 to 6 nm after heat treatment at 300–600 °C. All deposited films were X-ray amorphous up to 500 °C of heat treatment, above which a crystalline structure appeared. The crystallized composite film corresponded to the hexagonal structure of TT-Nb_2O_5.

Introduction

In view of the increasingly strict regulations for emissions from motor vehicles and heating systems, the need for modern, cost-effective and reliable sensors has been explored. In addition to conventional sensors based on the oxygen-ion conductor ZrO_2, sensors fabricated by the means of semiconducting oxygen-sensitive metal oxide films (TiO_2, Nb_2O_5, $SrTiO_3$, CeO_2, $SrSnO_3$) represent the most promising sensors for future applications.[1–4]

The behaviour of some oxygen-sensitive materials depends on the values of the partial pressure of oxygen. This leads to an ambiguous response of the sensors in specific applications, but the ambiguity can be avoided by selective incorporation of dopants. For example, it is reported that the Nb doped TiO_2 oxygen gas sensor shows higher sensitivity and shorter response times compared with pure TiO_2 sensors at significantly lower operating temperatures.[5]

Moreover, TiO_2-, SiO_2-, and Al_2O_3-supported platinum catalysts are used in several industrial processes.[6–8] In recent years, platinum has been widely employed as one of the most interesting noble metals because of its excellent chemical and physical properties. Even though a great number of studies have dealt with Pt/TiO_2 catalysts, the metallic surface characterization of Pt/Nb_2O_5 has not received much attention yet. Many techniques, such as radio frequency sputtering, ion-beam enhanced deposition and sol–gel methods have been used for the synthesis of thin films. The liquid phase deposition method (LPD) which has been developed and reported previously[9–12] is a wet process employed to prepare metal oxide thin films from aqueous solution at low temperatures (30–50 °C). Compared to vapor deposition techniques, the LPD method offers lower capital equipment costs (based on aqueous precursors), lower processing temperatures, lower shrinkage and flexibility in the choice of substrates with respect to topography and thermal stability. This technique is also used to incorporate dopants in thin films as precisely as possible.

In this paper, we report on the fabrication and characterization of Pt nanoparticles dispersed in Nb_2O_5 composite films by the LPD method. The characteristics of the deposited films are discussed on the basis of results obtained from X-ray diffraction (XRD), high-resolution transmission electron microscopy (HRTEM), X-ray photoelectron spectroscopy (XPS) and Fourier transform infrared spectroscopy (FT-IR).

Experimental

Niobium(v) oxide (Nb_2O_5; Taki Chemical Co. Ltd) powder and $NH_4F{\cdot}HF$ (Nacalai Tesque Inc.) aqueous solution were used for the thin film formation. The niobium source solution was obtained by dissolving Nb_2O_5 powder (7.4 g, 20 mmol) in $NH_4F{\cdot}HF$ (57.9 g, 1.0 mol) aqueous solution (1000 ml). Boric acid (H_3BO_3) was used as a F^- scavenger. Tetraammineplatinum chloride ($Pt(NH_3)_4Cl_2$) solution was prepared as a platinum precursor. Various substrates were employed depending on the needs of the different characterization techniques. For the XRD measurements, the composite films were deposited on non-alkali glass (Corning 7059). Si (111) wafers were used as substrates for the XPS and FT-IR experiments. For the TEM cross-sectional observations, the composite films were deposited on gold wire. After being degreased and washed ultrasonically, the substrates were immersed in the mixed solution and suspended therein vertically for 40 h at 30 °C in a constant temperature water bath. The mixed solution contains a niobium source solution at a concentration of 4.0 mM (1 M = mol dm^{-3}), 0.2 M H_3BO_3 and 0.6 mM $Pt(NH_3)_4Cl$. Once the reaction was finished, the substrates were removed and washed with deionized water. The samples were dried at ambient temperature. The deposited films were pre-treated at 100, 200, 300, 400, 500 and 600 °C in an airflow for 1 h before being removed for spectroscopic and microscopic observations.

The phases and the crystallographic structures of the deposited films were determined by XRD measurements on a Rigaku RINT-2100 diffractometer equipped with a thin film attachment using Cu Kα radiation. The incident angle of the X-rays to the sample was 1 degree. XPS analyses were carried out on a Kratos XSAM 800 with Mg Kα radiation (1253.6 eV) for the determination of the oxidation state and the chemical structure of materials. The C 1s peak (284.6 eV) was used as reference for the correction of the XPS positions of the obtained films. TEM images, which were obtained using a

JEOL JEM-2010 at acceleration voltage of 200 kV, were used to observe the morphology and size of particles in the composite films. For the cross-sectional HRTEM observations, the composite film was deposited on gold wire. After deposition, the film was dipped in an epoxy matrix followed by curing at room temperature for 72 h. Thin cross sections with thickness of 20 to 40 nm were obtained by sectioning with a Leica Ultra cut UCT using a diamond knife. For plan-view TEM observations, a thin carbon coating was used on the deposited film formed on the glass substrate, in order to prevent charging up effects by electron beams during observation. Then, the sample was exposed to diluted hydrogen fluoride vapour for 30 s. The deposited film was separated from the substrate by floating in the water bath and put onto a perforated carbon foil supported on a copper grid. The infrared spectra of the films were recorded with a FT/IR615 (JASCO) spectrometer equipped with a RAS attachment (PR-510, JASCO) in the range of 650–3650 cm^{-1}. The resolution and incident angle were 2 cm^{-1} and 65°, respectively.

Results and discussion

The crystal structure of most Nb_2O_5 phases is mainly composed of octahedra with niobium atoms in the centre, surrounded by six oxygen atoms. The structure is similar to that of ReO_3 which is an orthogonal package of oxygen octahedra. Each oxygen atom is shared with one neighboring octahedron. A great variety of polymorphs can be obtained by different arrangements of the sharing planes.[13,14] Many investigations into the crystal structure of the Nb_2O_5 polymorphs are available in the literature, unfortunately without giving any definitive picture of all the phases. The different Nb_2O_5 phases strongly depend on the method of preparation and annealing conditions.

The principal low temperature form, the orthorhombic T form, is reported to crystallize between 500 and 800 °C. A pseudohexagonal phase, the TT form, is also observed at lower temperatures. The TT phase changes continuously toward the T phase when subjected to higher temperature. The T and TT phases were named by German workers and signify the low- (tief) and very-low- (tief-tief) temperature forms of Nb_2O_5.[15] All reflections of the TT phase correspond to one or a pair of closely spaced reflections of the T phase. Thus, the TT phase is believed to be a poorly crystallized state of the T phase because of the similarity of their structures.

The transition temperatures strongly depend on the initial chemical composition, the structure of the compound and the conditions of annealing (time and rate of heating atmosphere). The glass substrates begin to melt above 600 °C. Therefore, we discuss heat treatment temperatures between 100 and 600 °C. The obtained deposited films are a light transparent yellow color in the as-deposited state and gradually change to brown after heat treatment at 600 °C. These color changes are indicative of the formation of Pt particles in the deposited films. The color can be related to the crystallite (the degree of crystallinity) of the film.

Fig. 1 shows the X-ray diffraction pattern of the deposited films, as-deposited and heat-treated at different temperatures. The deposited films exhibit an amorphous nature, *i.e.*, no discernible diffraction peaks are observed up to 500 °C. At 600 °C, diffraction peaks (indicating the crystallinity) appear approximately at $2\theta = 22.6°$, 28.6° and 36.8° (shown with black circles in the figure) assigned to the hexagonal TT-Nb_2O_5 phase (JCPDS 28–317 data). Furthermore, two sharp diffraction peaks are observed approximately at $2\theta = 39.8°$ and 46.4° (shown by white circles in the figure) attributed to the (111) and (200) reflection lines of the cubic structure of Pt, respectively.

FT-IR spectra of the deposited films with various heat treatment temperatures are shown in Fig. 2. We emphasize the

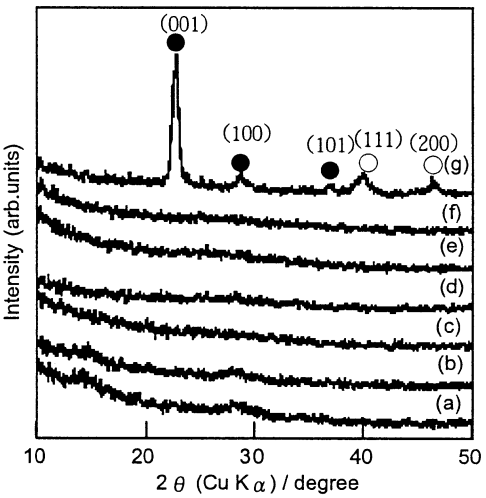

Fig. 1 XRD patterns of the Pt/Nb_2O_5 composite films with various heat treatment temperatures: (a) as-deposited film, (b) to (g); films heat-treated at 100–600 °C, respectively. ●: Nb_2O_5, ○: Pt.

regions of change indicated by arrows in Fig. 2. All deposited films show the main bands in the range of 650 to 1000 cm^{-1} which are attributed to Nb–O stretching, Nb–O–Nb bridging and Nb_3–O stretching modes. The bands at 1400 and 1540 cm^{-1} and the broad one at 2800–3700 cm^{-1} are assigned to the O–H and N–H vibrations for the water molecules and NH_4^+ ions, respectively.[16] Since the LPD process is performed in an aqueous solution system, water molecules can be readily absorbed and adsorbed by the film. NH_4^+ ions which are contained in the niobium source solution are enclosed in the deposited oxide film during the reaction. These O–H and N–H vibration bands completely disappear after treatment above 200 °C.

The Pt 4f core-level spectra for the deposited films with various heat treatment temperatures are shown in Fig. 3. These spectra are recorded at room temperature and show a typical doublet structure (Pt $4f_{5/2}$ and Pt $4f_{7/2}$) due to spin–orbit splitting. For the as-deposited film, the Pt $4f_{7/2}$ peak is observed at 72.6 eV and assigned to the Pt^{II} ionic state. This indicates that the Pt is situated in the niobium oxide matrix as an ionic state in the as-deposited film. The peak position of Pt $4f_{7/2}$ shifts to lower energy with increasing temperatures. The peak-fitted Pt 4f core line spectra for a film treated at 300 °C are shown in Fig. 4. The fitting of Pt 4f exhibits two binding

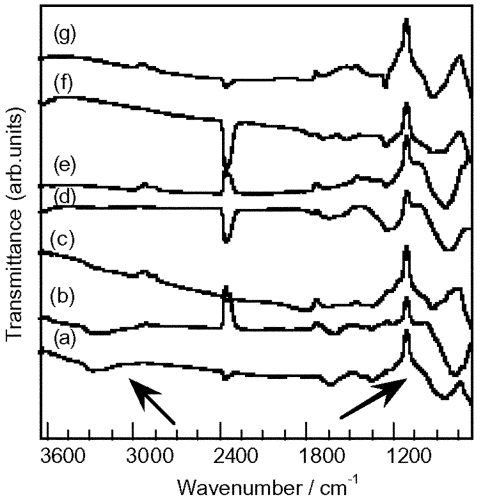

Fig. 2 FT-IR spectra of the Pt/Nb_2O_5 composite films heat-treated at various temperatures: (a) as-deposited film, (b) to (g); films heat-treated at 100–600 °C, respectively.

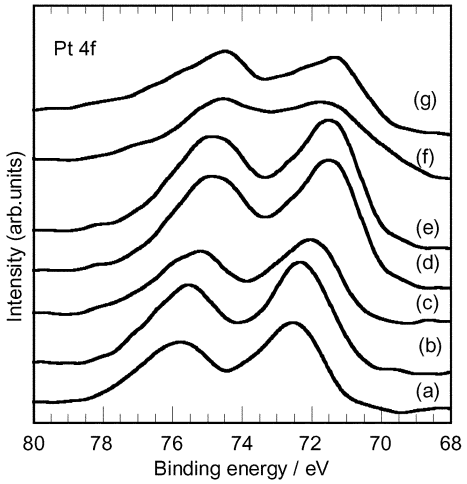

Fig. 3 Evolution of the Pt 4f electron spectra of the Pt/Nb_2O_5 composite films heat-treated at various temperatures: (a) as-deposited film, (b) to (g); films heat-treated at 100–600 °C, respectively.

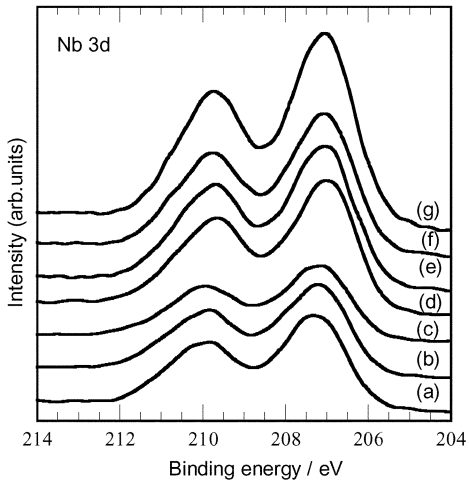

Fig. 5 Evolution of the Nb 3d electron spectra of the Pt/Nb_2O_5 composite films heat-treated at different temperatures: (a) as-deposited film, (b) to (g); films heat-treated at 100–600 °C, respectively.

energies for Pt $4f_{7/2}$ at 72.6 and 71.2 eV. These values represent the Pt^{II} ionic state and the metallic Pt (Pt^0) state, respectively.[17] For the films treated at 500 and 600 °C, the spectra become sharpened and the Pt $4f_{7/2}$ peaks are observed near 71.0 eV (Fig. 3). According to these results, the partial reduction of Pt^{II} ionic species in the deposited films is expected to be observed after treatment at 200 °C and reduction may be complete at about 500 °C.

The reduction of Pt ionic species may not occur without the decomposition of $[Pt(NH_3)_4]^{2+}$ ionic species. Therefore, it is considered that $[Pt(NH_3)_4]^{2+}$ ionic species are decomposed between 200 and 300 °C in the airflow as follows:

$$[Pt(NH_3)_4]^{2+} \rightarrow Pt^{2+} + 4NH_3\ (g) \uparrow \quad (1)$$

The generated electrons from the evaporation of ammonia gas are trapped and the Pt^{II} ionic species in the deposited film are reduced to the Pt^0 state by these electrons according to:

$$Pt^{2+} + 2e^- \rightarrow Pt^0 \quad (2)$$

$$nPt^0 \rightarrow (Pt^0)_n \quad (3)$$

Pt atoms produced as in eqn. (2) may tend to aggregate to form the Pt nanocrystal as shown in eqn. (3).

Figs. 5 and 6 show the core level XPS spectra of Nb 3d and O 1s peaks for the deposited films with various heat treatment temperatures. For all deposited films (Fig. 5), a pair of peaks due to the Nb $3d_{3/2}$ and Nb $3d_{5/2}$ core levels is observed at binding energies of 210.3 and 207.5 eV. These values correspond to the Nb^{5+} ionic state and suggest that the deposited films are niobium(v) oxide. A broad O 1s spectrum with an asymmetric profile is observed for the as-deposited film and this may be connected with the presence of hydroxy groups and adsorbed water molecules (Fig. 6a). However, the O 1s peaks become sharp on treatment above 200 °C. It indicates the elimination of water from the film due to heat treatment. The corresponding O 1s peaks of all the deposited films are centred on 530.2 eV and can be assigned to the O^{2-} constituent of the Nb_2O_5 film.[18]

The morphology of the deposited films and the mean sizes of Pt particles are directly observed by plan-view TEM observation. Fig. 7 shows top-view TEM images of the deposited films treated at 300 to 600 °C. It can be clearly observed that the number of Pt particles increases with increasing temperatures. Fig. 8 shows the size distribution patterns of the Pt particles shown in Fig. 7. A part of the micrograph field, including more than 200 particles, is randomly selected to analyze the size distribution. In Figs. 7 and 8, the size distribution patterns shown in (a), (b) and (c) have average diameters of 2.0, 2.3 and

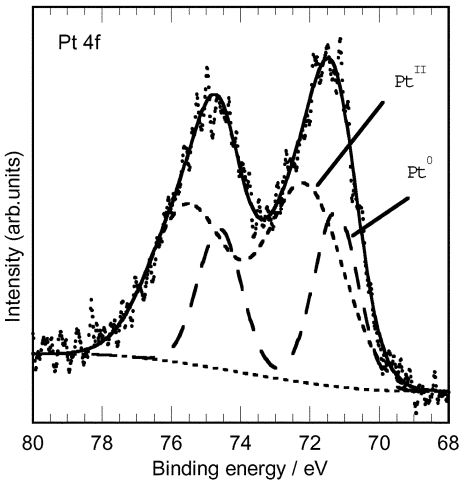

Fig. 4 Pt 4f electron spectrum of the Pt/Nb_2O_5 composite films heat-treated at 300 °C: (···) measured, (- - -) Pt^{II}, (– – –) Pt^0 component, and (—) fitted curve.

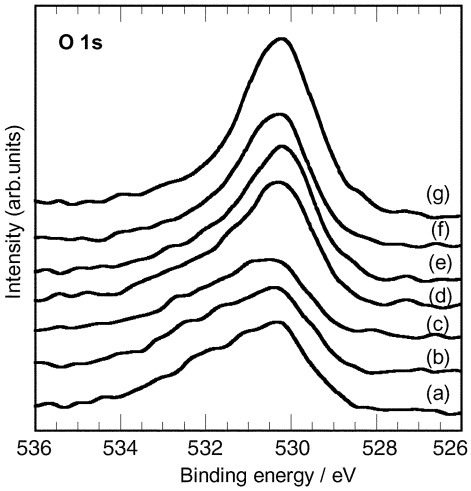

Fig. 6 Evolution of the O 1s electron spectra of the Pt/Nb_2O_5 composite films heat-treated at various temperatures: (a) as-deposited film, (b) to (g); films heat-treated at 100–600 °C, respectively.

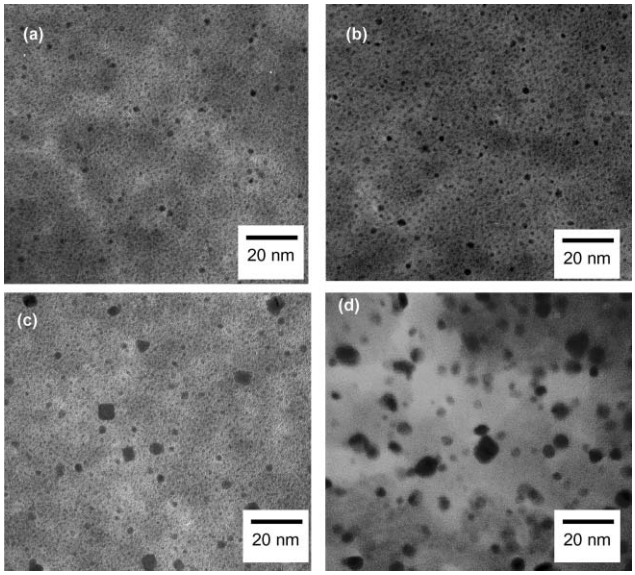

Fig. 7 Plan-view HRTEM images of the Pt/Nb_2O_5 composite films heat-treated at (a) to (d): 300, 400, 500 and 600 °C, respectively.

2.5 nm, respectively, with a standard deviation of 0.4 nm while (d) has a diameter of 5.6 nm with a standard deviation of 0.6 nm. The size distributions become sharper with increasing temperatures.

The HRTEM plan-view images of the films, as-deposited and heat-treated at 600 °C, are depicted in Fig. 9. The corresponding selected-area electron diffraction (SAED) patterns are shown in the inset. The as-deposited composite film shows a featureless amorphous state. The SAED pattern demonstrates a diffuse halo, due to the presence of the amorphous phase of Nb_2O_5 (Fig. 9a). On the other hand, diffraction rings and bright spots are observed in the SAED pattern for the film heat-treated at 600 °C (Fig. 9b). The Debye–Scherrer rings illustrate polycrystalline Nb_2O_5 and the spots refer to single crystalline Pt.

It can clearly be observed that spherical Pt particles (with mean sizes of 2 to 6 nm) dispersed in the film are mostly single crystal and distributed around the Nb_2O_5 nanocrystalline

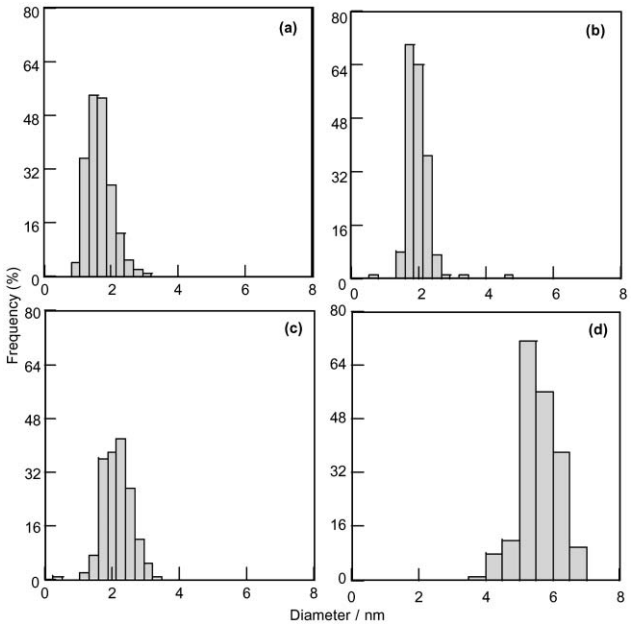

Fig. 8 Particle size distributions of dispersed Pt particles in the deposited films heat-treated at (a) to (d): 300, 400, 500 and 600 °C, respectively. The histograms were obtained from TEM images shown in Fig. 7(a)–(d). Mean particle size: 2.0, 2.3, 2.5, and 5.6 nm.

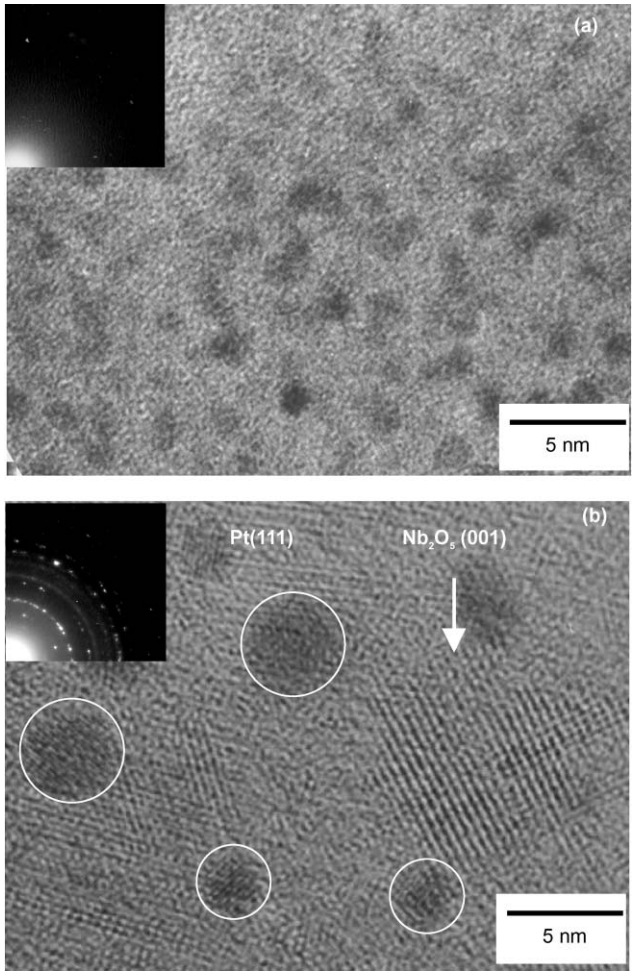

Fig. 9 Plan-view HRTEM images of the Pt/Nb_2O_5 composite films: (a) as-deposited film and (b) film heat-treated at 600 °C, respectively. The circles denote Pt nanocrystals and the arrow indicates the Nb_2O_5 nanocrystals formed in the film. Insets in (a) and (b) show the corresponding SAED patterns.

particles. High-resolution observation reveals that the lattice spacing is 0.23 nm which correspond to Pt (111) plane (circles in Fig. 9b). The lattice fringe corresponding to Nb_2O_5 (001) plane (with 0.41 nm spacing) is indicated by the arrow in Fig. 9b. The Nb_2O_5 nanocrystalline particles (nearly 10 nm) are observed throughout the entire deposited film. These results signify that the heat treatment not only causes the reduction of Pt^{II} ionic species to Pt particles but also involves the crystallization of the Nb_2O_5 matrix.

Figs. 10a and 10b show the cross-sectional HRTEM images of the deposited films, as-deposited and heat-treated at 600 °C. The as-deposited film exhibits an amorphous nature (Fig. 10a). In contrast, the spherical Pt particles are homogeneously dispersed into the Nb_2O_5 matrix after treatment at 600 °C (Fig. 10b). The thickness of the composite film is approximately 80 nm. The size of Pt particles is quite similar to those in the plan-view image (Fig. 9b). It follows from these results that Pt nanoparticles are distributed not only on the surface but also inside of the composite film.

Conclusions

Highly-dispersed 2–6 nm Pt nanoparticles containing Nb_2O_5 composite films have been fabricated by the LPD method. This is a simple process for the preparation of composite oxide thin films. The Nb_2O_5 thin films containing Pt ionic species are deposited from a mixed solution of niobium source, H_3BO_3 acid, and $Pt(NH_3)_4Cl_2$ aqueous solutions under the ambient

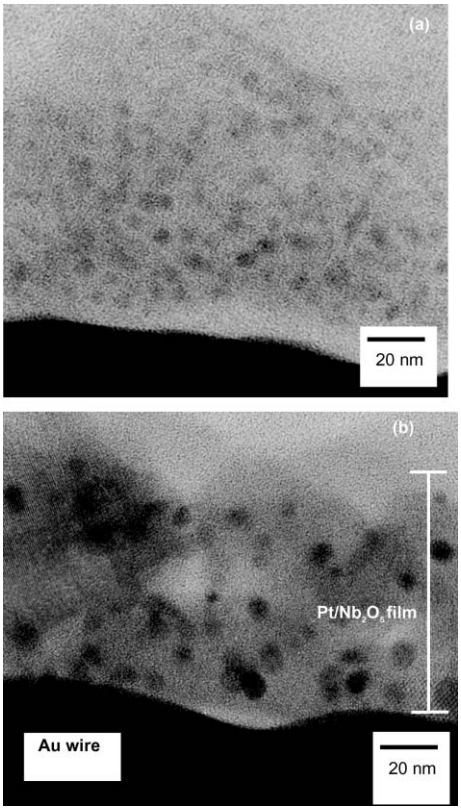

Fig. 10 Cross-sectional HRTEM images of the Pt/Nb_2O_5 composite films deposited on gold wire: (a) as-deposited film and (b) film heat-treated at 600 °C, respectively.

temperature. The Pt^{II} ionic species are reduced to metallic Pt particles after heat treatment above 200 °C. The dispersion of Pt particles into the Nb_2O_5 matrix is homogeneous. The size of the dispersed Pt particles can be controlled by heat treatment. All the deposited films are X-ray amorphous up to temperatures of 500 °C, above which a crystalline structure appears. The crystallized composite film corresponds to the hexagonal structure of TT-Nb_2O_5.

Acknowledgement

This work was partly supported by Grants-in-Aid for Scientific Research No. 12305056 from the Ministry of Education, Science, Sports and Culture, Japan.

References

1 R. K. Sharma, M. C. Bhatnagar and G. L. Sharma, *Sens. Actuators B*, 1998, **46**, 194.
2 H. J. Beie and A. Gnorich, *Sens. Actuators B*, 1994, **4**, 393.
3 U. Lampe, M. Fleischer and H. Meixner, *Sens. Actuators B*, 1994, **17**, 187.
4 H. Meixner, J. Gerblinger and M. Fleischer, *Sens. Actuators B*, 1993, **15–16**, 45.
5 M. Z. Atashbar, H. T. Sun, B. Gong, W. Wlodarski and R. Lamb, *Thin Solid Films*, 1998, **326**, 238.
6 F. Pesty, H. Steinruck and T. E. Madey, *Surf. Sci.*, 1995, **339**, 83.
7 G. Szollosi, B. Torok, G. Szakonyi, I. Kun and M. Bartok, *Appl. Catal. A*, 1998, **172**, 225.
8 K. Kohno, Y. Takeda, N. Imanishi, Y. Sakaki, K. Sakamoto and O. Yamamoto, *J. Am. Ceram. Soc.*, 1993, **76**, 192.
9 H. Nagayama, H. Honda and H. Kawahara, *J. Electrochem. Soc.*, 1988, **135**, 2013.
10 A. Hishinuma, T. Goda, M. Kitaoka, S. Hayshi and H. Kawahara, *Appl. Surf. Sci.*, 1991, **48**(49), 405.
11 S. Deki and Y. Aoi, *J. Mater. Res.*, 1998, **13**, 883.
12 S. Deki, Y. Aoi, H. Yanagimoto, K. Ishii, K. Akamatsu, M. Mizuhata and A. Kajinami, *J. Mater. Chem.*, 1996, **6**, 1879.
13 E. I. Ko and J. G. Weissman, *Catal. Today*, 1990, **8**, 27.
14 D. Rosenfeld, R. Sanjines, F. Levy, P. A. Buffat, V. Demarne and A. Grisel, *J. Vac. Sci. Technol. A*, 1994, **12**, 135.
15 J. G. Weissman, E. I. Ko and P. Wynblatt, *J. Catal.*, 1987, **108**, 383.
16 M. Macek, B. Orel and U. O. Krasovec, *J. Electrochem. Soc.*, 1997, **144**, 3002.
17 M. Peuckert and H. P. Bonzel, *Surf. Sci.*, 1984, **145**, 239.
18 N. Kumagai, K. Tanno, T. Nakajima and N. Watanabe, *Electrochim. Acta*, 1983, **28**, 17.